Unravelling the chemistry of the [Cu(4,7-dichloroquinoline)$_2$Br$_2$]$_2$ dimeric complex through structural analysis: a borderline ligand field case

Giada Finocchio,[a] Silvia Rizzato,[a] Giovanni Macetti,[b] Gers Tusha,[a] and Leonardo Lo Presti[a,*]

[a] Department of Chemistry, Università degli Studi di Milano, Via Golgi 19, 20133 Milano (Italy)
[b] Laboratoire de Physique et Chimie Théoriques, Université de Lorraine and CNRS, 1 Boulevard Arago, Metz, F-57078, France

* To whom correspondence should be addressed: leonardo.lopresti@unimi.it

SUPPORTING INFORMATION

INDEX

Section S1. Multipole model 3
S1.1 Disorder 3
S1.2 Anharmonicity 3
S1.3 Strategy of multipole refinement 4
S1.4 Bulk quantum simulations 5
S1.5 Least–squares results 6
Section S2. Crystal packing 16
S2.1 Atom–atom contacts 16
S2.2 Stacking motifs 17
Section S3. Geometry 19
S3.1 Coordination and relative ligand orientation 19
S3.2. DFT–optimized geometries 20
Section S4. Chemical bonding 23
S4.1 Aromaticity of 4,7–dichloroquinoline 25
Section S5. Magnetic susceptivity measurement 27
Section S6. DFT electronic structure 28

Section S1. Multipole model

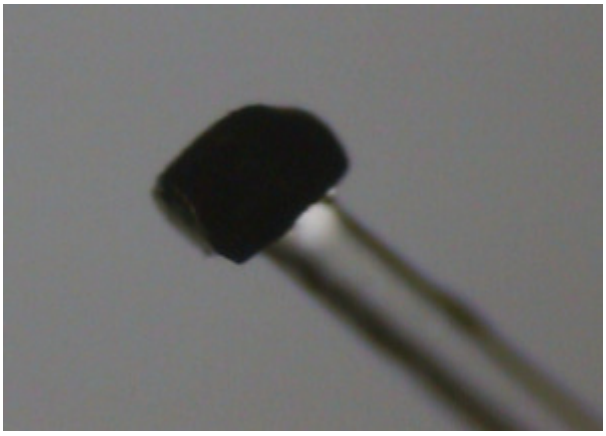

Figure S1. The X-ray quality crystal employed to perform the X-ray analysis at 100 K, mounted on the top of a capillary fiber with a drop of bi–component epoxy glue. The habit is prismatic, with main dimensions of ~ 0.350 x 0.225 x 0.200 mm.

S1.1 Disorder

Occupational disorder is present at the Br(1) site (see Figure 1 in the main text), with a site occupation factor (s.o.f.) estimated as large as 0.8870(6) at 100 K by the Independent Atom Model (IAM). Analysis of Fourier residuals around terminal atoms of preliminary multipole models confirms this view, which implies that ~11 % of the coordination sites lack of one bromine ligand (see text). The disorder has been explicitly dealt with by the multipole model by setting the s.o.f. of Br(1) at the IAM estimate.

S1.2 Anharmonicity

Residual anharmonic motion persists in organic crystals well below the room temperature.[1] Accordingly, the explicit introduction of anharmonicity in the model, where allowed by the data, is a fundamental prerequisite for obtaining an accurate electronic density.[2] In CDCQB, "shashlik-like" Fourier residuals,[3] characterized by an alternation of positive and negative features, appear close to halogen atoms at 100 K, even when the multipole model is applied (Figures S2a,c–S3a). These features neatly disappear when third–order Gram–Charlier coefficients[4] are added (Figure S2b,d–S3b). Our maximum data resolution (1.0 $Å^{-1}$) fulfills the Kuhs[5] rule of thumb for significance of anharmonic refinement up to the third–order (1.06 $Å^{-1}$ for the present dataset), allowing us to refine C^{ijk} parameters with reasonable confidence.

CDCQB bears two independent 4,7–dichloroquinoline in the asymmetric unit (see Figure 1 in the main text). Interestingly, chlorine atoms of one molecule are less affected by anharmonicity than those of the other one (Figure S2, compare panels in columns (c) and (a)). The same is true also for bromine ligands: moreover, some residual features are still detectable in the Fourier map close to Br(1) after the addition of third–order Gram–Charlier coefficients (Figure S3). However, due to the contemporary occurrence of disorder at this site, it is difficult to understand whether they are due to some kind of residual anharmonicity. Addition of fourth–order coefficient is not advisable, due to the limit of the Kuhs rule.

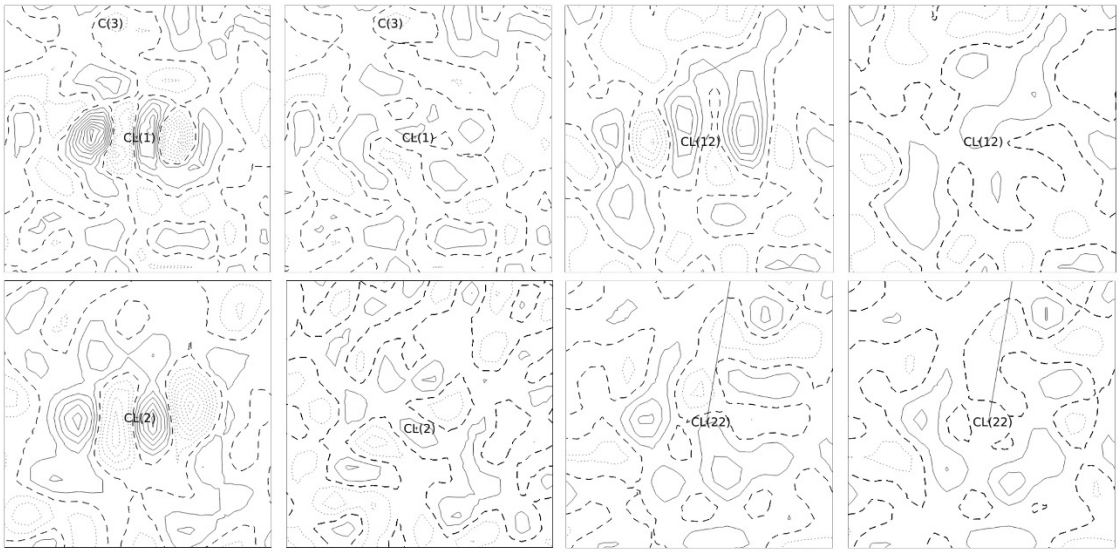

Figure S2. 1.7 x 1.7 Å isocontour maps of Fourier residuals around chlorine atoms in CDCQB at 100 K. The multipole models includes expansions up to *l*=2 for H, *l*=3 for C, N and *l*=4 for Cu, Cl and Br, with radial parameters equal to their default values, and differ only for the treatment of thermal motion. Full lines: positive values. Dashed lines: 0 level. Dotted lines: negative values. Isocontours are drawn at step of 0.1 eÅ^{-3}. (a) Cl(1) and Cl(2), only harmonic. (b) Cl(1) and Cl(2), third–order Gram–Charlier coefficients added. (c) Cl(12) and Cl(22), only harmonic. (d) Cl(12) and Cl(22), third–order Gram–Charlier coefficients added.

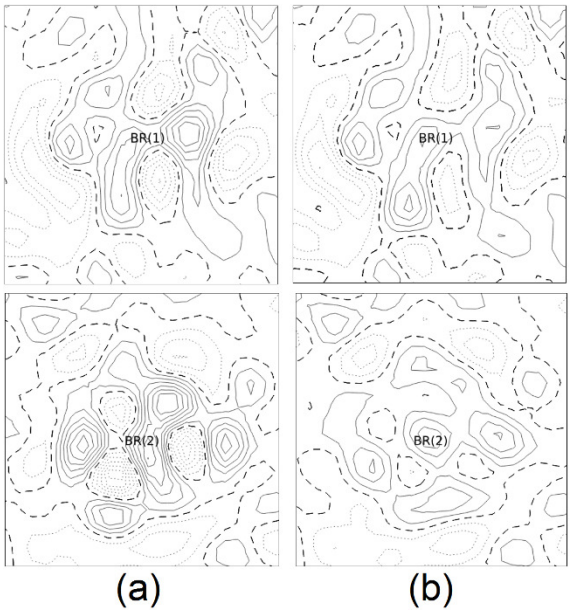

Figure S3. Same as Figure S2 above, for the two symmetry–independent Br(1) and Br(2) atoms. (a) Br(1) and Br(2), only harmonic. (b) Br(1) and Br(2), third–order Gram–Charlier coefficients added.

S1.3 Strategy of multipole refinement

The final multipolar model has been obtained by a stepwise procedure, in which the model complexity has been increased progressively. Neither intensity nor significance cutoffs have been applied to the dataset of diffraction amplitudes. In fact, there is no physical justification for applying arbitrary cutoffs on otherwise good–quality data. As high–order reflections are intrinsically weaker than low resolution ones, any arbitrary cutoff implies a significant loss of information in high–order

regions of the reciprocal space. Even though, from a statistical point of view, fewer weak data imply lower crystallographic agreement factors, it is difficult to estimate the systematic error associated to the loss of information. To the best of our knowledge, no systematic studies even exist on the influence of this problem on the quality of the resulting multipole model. In this work, we refine model parameters against all the observed data (F(hkl)> 0), regardless of their absolute intensity, even if this strategy implies a slight worsening of the statistical agreement factors.

The least–squares procedure has relied on a full set of 15521 symmetry–independent observed (F(hkl) >0) diffraction amplitudes collected at T = 100 K up to $\sin\theta/\lambda = 1.00$ Å^{-1} (Table 1 in the main text). Four low–order reflections [(2 -9 4), (-5 7 5), (5 -8 7) and (-6 -1 7)] have been marked as outliers by PLATON, likely due to absorption overcorrection, and have been thus excluded from the dataset. Due to surface roughness and black crystal color (Figure S1), applying a reliable analytical correction was impossible. However, including or not these outliers out of 15521 symmetry-independent reflections in the data set do not change significantly the model outcomes.

C–H covalent bonds have been renormalized to the corresponding neutron estimates (1.083 Å) with Mercury, while anisotropic displacement parameters for hydrogen atoms have been estimated by the SHADE2.1 webserver. Coordinates and thermal parameters of hydrogen atoms have been kept fixed throughout. For all atoms, basis functions of Su and Coppens [6] have been employed, starting from orbital occupancies corresponding to neutral atoms (Cu: s^1d^{10}; Br and Cl: s^2p^5) and the valence contribution of atomic scattering factors has been attributed to the external electrons (Cu: 4s, 3d; Br: 4s, 4p; Cl: 3s, 3p; N, C: 2s, 2p; H: 1s). After preliminary refinements of atomic coordinates and anisotropic displacement parameters, multipole coefficients up to hexadecapoles (l=4) have been added progressively. Third–order Gram–Charlier coefficients have been used for all the halogen atoms, to model low–T anharmonicity (see below). Radial scaling parameters for each atomic specie have been refined only in the last stages of the procedure and kept frozen in the last refinement cycles. The final multipole expansions included electronic parameters up to quadrupoles (l=2) for H, octupoles (l=3) for C, N and hexadecapoles (l=4) for heavier Cl, Br and Cu atoms. For H atoms, only bond–directed l=1 poles (corresponding to z–components in the local atomic reference frame) have been considered, as other components were null within 1 estimated standard deviation. Moreover, Cu occupies a C_{2v} pseudo–symmetric site exploiting non–crystallographic symmetry (Figures 1 and 3 in the main text). Therefore, only even–order poles refine to values higher than zero. Accordingly, odd–order poles of Cu have been excluded from the final parameter set. Table 1 in the main text shows final radial scaling parameters for the different atomic species, while Tables S1–S8 summarize all the other least–squares variables.

At each step, as many parameters as possible have been refined together. Nevertheless, due to the contemporary occurring of disorder and anharmonicity, the model for charge density of CDCQB is quite complex. Thus, a block refinement strategy has been applied in the last stages of the procedure, to disentangle otherwise strongly correlated least–squares variables. Atomic positions, thermal motion parameters up to the third–order, electron population coefficients, and radial scaling factors have been repeatedly cycled until their changes became lower than their least–squares deviations. Eventually, no correlations higher than 0.75 have been achieved, the latter concerning third–order Grahm–Charlier coefficients on the Cl(2) chlorine.

Overall, the least–square multipole model against experimental structure factor amplitudes is satisfactory, in terms of agreement factors (Tables 1 in the main text and S1 below), residual systematic errors (Figure S2) and Fourier residuals (Figures S3–S4).

S1.4 Bulk quantum simulations

Single–point DFT simulations were also carried out on the experimental X–ray structure of the complex at 100 K with the CRYSTAL14 program, with the aim of providing static structure factor amplitudes for comparison with experimental ones. The geometry correspondent to the best multipole model has been employed. The same Hamiltonian and basis set used in the gas–phase simulations

have been exploited. Minnesota-class meta-GGA M06 functional, able to partly retrieve long–range dispersion effects, was exploited together with the triple zeta valence polarization (TZVP) basis set proposed by Peintinger for accurate solid state calculations. Truncation criteria of the Coulomb and exchange series were set to either 10^{-7} or 10^{-14} (TOLINTEG 7 7 7 7 14). A level shifter of either 0.7 h, as well as an 80% mixing of the Kohn−Sham matrix coefficients, have been applied to subsequent SCF cycles to accelerate convergence. A 6 × 6 × 6 sampling of the independent part of the first Brillouin zone was used to define the k-space grid to solve the SCF problem.

The idea is to provide an error–free benchmark for the charge density model of CDCQB. As X-ray structure factor amplitudes do not depend on the spin state of Cu atoms, only the diamagnetic solution (M_S=0) has been considered to develop the charge density model.

Moreover, quantum chemical calculations do not account for finite–T effects. Accordingly, atomic coordinates have been kept frozen to the experimental ones. Thermal motion parameters have been set to 0 and never refined. Radial scaling parameters have also been kept fixed at the default ones, which are indeed very similar to those refined against the experimental data (Table 1 in the main text). Finally, the multipole refinement has been carried out against structure factor amplitudes (F) rather than on their square modules (F^2). Apart these differences, the same multipolar model above described has been refined against both sets of theoretical structure factors. Table S1 shows the results, in comparison with the experiment–derived ones.

S1.5 Least–squares results

Table S1. Comparison of relevant agreement factors of multipole models developed against experimental structure factor amplitudes (F^2_{exp}), theoretical structure factors from the crystallographic cell model (F_{theo}).

	F^2_{exp}	F_{theo}
R(*F*)	0.0239	0.0030
R(F^2)	0.0209	0.0053
GOFw	1.011	0.031
Data–to–parameter ratio	28.1	28.1
$\Delta\rho$ /$e\cdot$Å^{-3}	–0.418, +0.497	–0.247, +0.330

Comment: Considering the magnitude of Fourier residual estimated in both multipole–projected quantum charge densities, which are clearly due to the multipole model bias, the experimental charge density is satisfactory and accurate. Figure S4 shows the corresponding normal probability plot, which proves that most of systematic errors have been corrected and the multipole–predicted structure factor amplitudes, F_c, are fully consistent with the observed ones (F_o). Some residual deviations are apparent on the negative quantile tails (Figure S4), likely due to some residual anharmonicity on the bromine atom Br(1) (Figure S3). The introduction of higher–order anharmonic coefficients on bromine ligands, however, is not advisable at this resolution,[5] also taking into account that anharmonicity and occupational disorder are strictly intertwined in CDCQB. In any case, Fourier residuals (Figures S5 and S6) are mostly featureless and almost completely random distributed throughout the unit cell. The largest $\Delta\rho$ features are close to heavy bromine atoms (see also Section S1.2 above), and in particular to Br(2) (+0.49 $e\cdot$Å^{-3}). However, the relative magnitude of these residuals is small (~ 1.4 %) with respect the total number of electrons of a bromine atomic basin (35 *e*). In proportion, the error considered acceptable for Fourier residuals when only C, H, N, O atoms are present (~ ±0.2 $e\cdot$Å^{-3}) corresponds to about 3 % of the total electron count.

Overall, taking into account the potential sources of error that may have affected the data if not properly accounted for (high absorption, high–T anharmonicity, and disorder), these results demonstrate that the multipole expansion here adopted is an acceptable description of the electronic density of this complex.

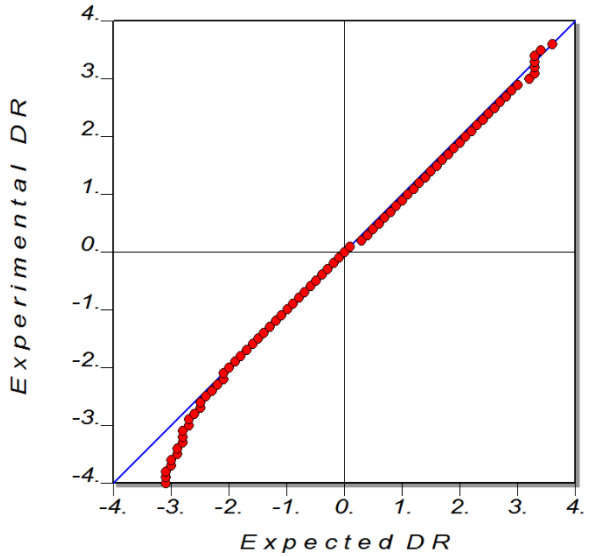

Figure S4. Normal probability plot of observed *vs*. expected dataset quantiles under the assumption that the measured structure factor amplitudes are subject only to random noise, that is, that (F_o–F_c) deviations *DR* are normally distributed.

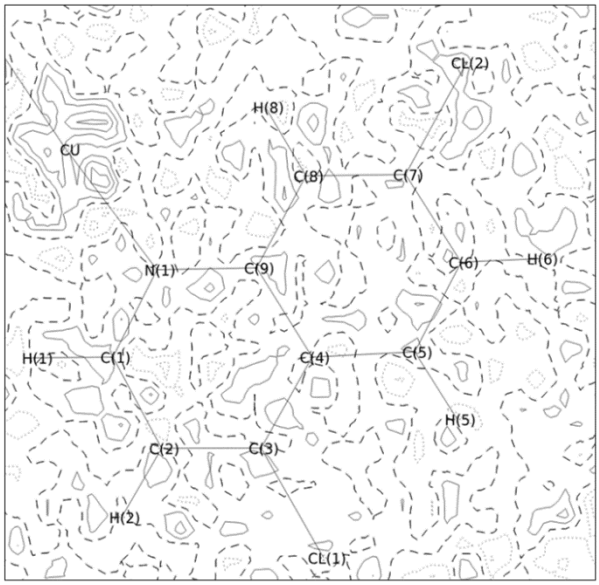

Figure S5. 3.8 Å x 3.7 Å (F_o–F_c) Fourier isocontour map up to $(\sin\theta/\lambda)_{max}$ = 1.0 $Å^{-1}$ for the best multipole model of CDCQB at 100 K in the plane of one of the 4,7–dichloroquinoline ligands, with the atom numbering scheme (see Figure 1 in the main text). Disorder and anharmonicity are included in the model. Full lines: positive values. Dashed lines: 0 level. Dotted lines: negative values. Isocontours at step of 0.1 $e \cdot Å^{-3}$.

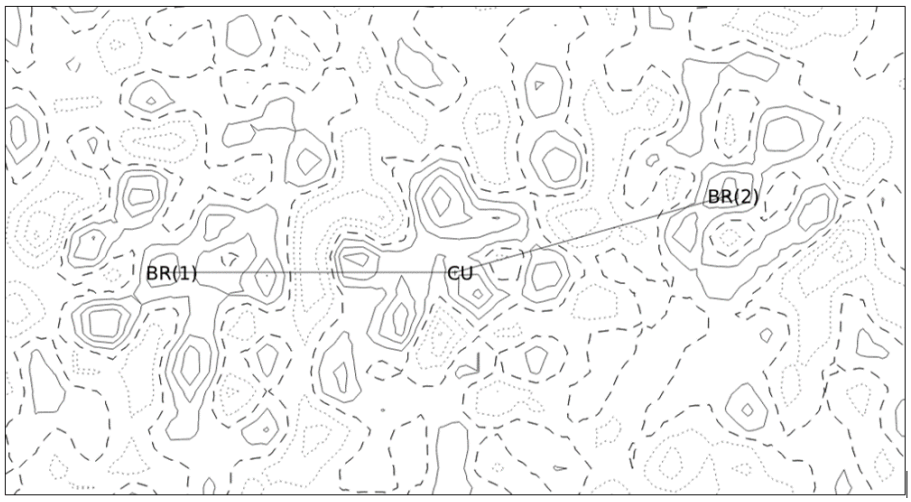

Figure S6. 3.6 Å x 1.9 Å Fourier difference map up to $(\sin\theta/\lambda)_{max}$ = 1.0 $Å^{-1}$, in the region of inner–sphere bromine ligands. Cu, Br(1) and Br(2) atoms all lie in the plane of the plot. Lines have the same meaning as in Figure S5 above.

Table S2. Coordinates and Uiso of CDCQB at T = 100 K

Atom	x	y	z	sof	U_{iso}
BR(1)	-0.12258(2)	0.87869(1)	0.47447(1)	0.8870	0.01279
BR(2)	0.41929(1)	0.91699(1)	0.29406(1)	1.0000	0.01833
CU	0.151169(8)	0.924941(6)	0.393095(6)	1.0000	0.01155
CL(1)	-0.19802(5)	1.32583(3)	-0.04016(3)	1.0000	0.03046
CL(12)	0.50980(4)	0.54697(3)	0.83426(3)	1.0000	0.02487
CL(2)	-0.25224(5)	0.69845(4)	0.11013(3)	1.0000	0.03182
CL(22)	0.10595(4)	0.45130(3)	0.32773(3)	1.0000	0.02253
N(1)	0.02997(6)	1.03897(5)	0.25433(4)	1.0000	0.01392
N(2)	0.27593(6)	0.80195(4)	0.52172(4)	1.0000	0.01427
C(1)	0.06612(9)	1.15389(6)	0.23991(5)	1.0000	0.01861
C(12)	0.35818(8)	0.84354(6)	0.60360(5)	1.0000	0.01779
C(2)	-0.0020(1)	1.2461(1)	0.1500(1)	1.0000	0.02199
C(22)	0.43503(8)	0.76646(6)	0.70133(5)	1.0000	0.01897
C(3)	-0.11227(9)	1.21620(6)	0.07124(5)	1.0000	0.01957
C(32)	0.42773(7)	0.64176(6)	0.71159(5)	1.0000	0.01698
C(4)	-0.15204(7)	1.09405(6)	0.08043(5)	1.0000	0.01610
C(42)	0.35281(7)	0.59126(5)	0.62192(5)	1.0000	0.01511
C(5)	-0.25826(8)	1.05607(7)	-0.00150(5)	1.0000	0.02067
C(52)	0.35426(8)	0.46230(6)	0.62124(5)	1.0000	0.01851
C(6)	-0.28837(8)	0.93594(8)	0.00829(5)	1.0000	0.02239
C(62)	0.28033(8)	0.41917(6)	0.53151(6)	1.0000	0.01978
C(7)	-0.21319(8)	0.84984(7)	0.10155(5)	1.0000	0.02004
C(72)	0.20197(7)	0.50560(5)	0.43955(5)	1.0000	0.01689
C(8)	-0.10970(8)	0.88247(6)	0.18328(5)	1.0000	0.01649
C(82)	0.19972(7)	0.63101(5)	0.43567(5)	1.0000	0.01522
C(9)	-0.07662(7)	1.00628(5)	0.17448(4)	1.0000	0.01362
C(92)	0.27572(7)	0.67654(5)	0.52728(5)	1.0000	0.01328
H(1)	0.15394	1.17804	0.30133	1.0000	0.03672
H(12)	0.36719	0.94156	0.59492	1.0000	0.03542
H(2)	0.03245	1.33842	0.14272	1.0000	0.04300
H(22)	0.49863	0.80449	0.76729	1.0000	0.03705
H(5)	-0.31654	1.12244	-0.07266	1.0000	0.03989
H(52)	0.41457	0.39672	0.69229	1.0000	0.03690
H(6)	-0.36862	0.90709	-0.05498	1.0000	0.04430
H(62)	0.28247	0.32053	0.53145	1.0000	0.03889
H(8)	-0.05412	0.81417	0.25387	1.0000	0.03195
H(82)	0.13975	0.69453	0.36315	1.0000	0.03008

Table S3. Harmonic anisotropic displacement parameters of CDCQB at T = 100 K.

	U11	U22	U33	U12	U13	U23
BR(1)	0.01500(2)	0.01159(2)	0.01166(2)	-0.00253(2)	-0.00087(2)	-0.00056(2)
BR(2)	0.01383(2)	0.02715(3)	0.01397(2)	-0.00422(2)	-0.00070(2)	-0.00142(2)
CU	0.01256(2)	0.01079(3)	0.01083(2)	-0.00248(2)	-0.00268(2)	0.00102(2)
CL(1)	0.0413(1)	0.0247(1)	0.0174(1)	0.0131(1)	-0.0038(1)	0.0051(1)
CL(12)	0.02362(7)	0.02815(8)	0.01747(6)	0.00289(6)	-0.00300(5)	0.00851(5)
CL(2)	0.0456(1)	0.0387(1)	0.0187(1)	-0.0296(1)	0.0027(1)	-0.0051(1)
CL(22)	0.02314(6)	0.01995(6)	0.02715(7)	-0.00587(5)	0.00367(5)	-0.00988(5)
N(1)	0.0168(2)	0.0132(2)	0.0110(2)	-0.0024(1)	-0.0027(1)	0.0010(1)
N(2)	0.0148(2)	0.0123(2)	0.0148(2)	-0.0019(1)	-0.0044(1)	0.0013(1)
C(1)	0.0291(3)	0.0137(2)	0.0125(2)	-0.0043(2)	-0.0041(2)	0.0014(2)
C(12)	0.0190(2)	0.0153(2)	0.0181(2)	-0.0025(2)	-0.0083(2)	0.0011(2)
C(2)	0.0376(3)	0.0133(2)	0.0133(2)	-0.0011(2)	-0.0030(2)	0.0015(2)
C(22)	0.0188(2)	0.0197(3)	0.0169(2)	-0.0014(2)	-0.0069(2)	0.0012(2)
C(3)	0.0261(3)	0.0168(2)	0.0120(2)	0.0057(2)	-0.0015(2)	0.0018(2)
C(32)	0.0147(2)	0.0180(2)	0.0154(2)	0.0010(2)	-0.0018(2)	0.0040(2)
C(4)	0.0142(2)	0.0213(2)	0.0106(2)	0.0023(2)	-0.0016(1)	0.0001(2)
C(42)	0.0138(2)	0.0137(2)	0.0155(2)	0.0008(2)	0.0011(1)	0.0034(2)
C(5)	0.0147(2)	0.0326(3)	0.0129(2)	0.0002(2)	-0.0033(2)	-0.0007(2)
C(52)	0.0187(2)	0.0132(2)	0.0209(2)	0.0007(2)	0.0039(2)	0.0042(2)
C(6)	0.0169(2)	0.0379(4)	0.0139(2)	-0.0090(2)	-0.0018(2)	-0.0038(2)
C(62)	0.0211(2)	0.0116(2)	0.0256(3)	-0.0016(2)	0.0056(2)	0.0003(2)
C(7)	0.0201(2)	0.0301(3)	0.0128(2)	-0.0125(2)	0.0009(2)	-0.0032(2)
C(72)	0.0159(2)	0.0131(2)	0.0217(2)	-0.0023(2)	0.0037(2)	-0.0027(2)
C(8)	0.0188(2)	0.0203(2)	0.0114(2)	-0.0071(2)	-0.0011(2)	-0.0012(2)
C(82)	0.0150(2)	0.0123(2)	0.0179(2)	-0.0013(2)	-0.0007(2)	-0.0013(2)
C(9)	0.0132(2)	0.0165(2)	0.0103(2)	-0.0013(2)	-0.0010(1)	-0.0001(1)
C(92)	0.0126(2)	0.0114(2)	0.0147(2)	-0.0006(1)	-0.0009(1)	0.0011(1)
H(1)	0.0522	0.0326	0.0276	-0.0159	-0.0126	-0.0013
H(12)	0.0453	0.0215	0.0395	-0.0083	-0.0135	-0.0004
H(2)	0.0731	0.0206	0.0348	-0.0105	-0.0049	0.0018
H(22)	0.0407	0.0401	0.0306	-0.0075	-0.0155	-0.0045
H(5)	0.0358	0.0523	0.0255	0.0034	-0.0116	0.0052
H(52)	0.0427	0.0263	0.0350	0.0025	-0.0024	0.0110
H(6)	0.0396	0.0698	0.0283	-0.0229	-0.0104	-0.0076
H(62)	0.0486	0.0174	0.0498	-0.0044	0.0049	-0.0024
H(8)	0.0422	0.0283	0.0242	-0.0090	-0.0067	0.0047
H(82)	0.0351	0.0261	0.0267	-0.0021	-0.0089	0.0018

Table S4. Third-order Grahm–Charlier coefficients of halogen atoms at 100 K.

Atom	C111	C222	C333	C112	C122	C113	C133	C223	C233	C123
Br(1)	0.000015	0.000002	-0.000023	0.000081	0.000036	0.000025	-0.000026	-0.000021	-0.000010	0.000018
Br(2)	-0.000079	0.000242	0.000013	0.000059	-0.000277	-0.000003	0.000025	-0.000040	-0.000001	-0.000032
Cl(1)	-0.002282	-0.000355	0.000127	-0.001455	-0.000800	0.000353	-0.000024	0.000117	0.000069	0.000182
Cl(12)	-0.000192	0.000320	-0.000001	0.000315	0.000375	0.000182	0.000080	-0.000009	-0.000106	0.000110
Cl(2)	0.004995	-0.000788	-0.000028	-0.002483	0.001294	-0.000080	0.000035	0.000004	-0.000013	0.000016
Cl(22)	0.000560	0.000133	0.000098	0.000035	-0.000087	-0.000076	0.000105	-0.000112	0.000027	0.000013

Table S5. Monopole Populations, Radial Parameters and Net Atomic Charges.

Atom	Pval	Kappa	P00	Kappa'	Atomic charge
BR(1)	8.600(44)	1.052	0.000	1.123	-1.600(44)
BR(2)	7.623(42)	1.052	0.000	1.123	-0.623(42)
CU	10.991(16)	1.004	0.000	1.012	+0.009(16)
CL(1)	7.216(36)	1.020	0.000	0.986	-0.216(36)
CL(12)	7.245(36)	1.020	0.000	0.986	-0.244(36)
CL(2)	7.213(37)	1.020	0.000	0.986	-0.212(37)
CL(22)	7.447(36)	1.020	0.000	0.986	-0.447(36)
N(1)	5.022(31)	1.004	0.000	0.903	-0.021(31)
N(2)	5.038(31)	1.004	0.000	0.903	-0.037(31)
C(1)	3.963(58)	1.013	0.000	0.952	+0.036(58)
C(12)	3.817(57)	1.013	0.000	0.952	+0.183(57)
C(2)	3.976(63)	1.013	0.000	0.952	+0.024(63)
C(22)	3.791(59)	1.013	0.000	0.952	+0.209(59)
C(3)	3.990(47)	1.013	0.000	0.952	+0.010(47)
C(32)	3.876(45)	1.013	0.000	0.952	+0.123(45)
C(4)	3.790(48)	1.013	0.000	0.952	+0.209(48)
C(42)	4.062(48)	1.013	0.000	0.952	-0.062(48)
C(5)	3.957(62)	1.013	0.000	0.952	+0.043(62)
C(52)	3.941(61)	1.013	0.000	0.952	+0.058(61)
C(6)	3.828(64)	1.013	0.000	0.952	+0.172(64)
C(62)	3.982(61)	1.013	0.000	0.952	+0.018(61)
C(7)	3.910(46)	1.013	0.000	0.952	+0.089(46)
C(72)	3.938(46)	1.013	0.000	0.952	+0.061(46)
C(8)	3.809(58)	1.013	0.000	0.952	+0.190(58)
C(82)	3.949(57)	1.013	0.000	0.952	+0.051(57)
C(9)	4.008(44)	1.013	0.000	0.952	-0.007(44)
C(92)	4.002(44)	1.013	0.000	0.952	-0.001(44)
H(1)	0.813(34)	1.230	0.000	1.133	+0.186(34)
H(12)	0.843(33)	1.230	0.000	1.133	+0.156(33)
H(2)	0.791(36)	1.230	0.000	1.133	+0.209(36)
H(22)	0.767(33)	1.230	0.000	1.133	+0.233(33)
H(5)	0.827(35)	1.230	0.000	1.133	+0.172(35)
H(52)	0.903(33)	1.230	0.000	1.133	+0.097(33)
H(6)	0.844(36)	1.230	0.000	1.133	+0.155(36)
H(62)	0.808(34)	1.230	0.000	1.133	+0.191(34)
H(8)	0.805(32)	1.230	0.000	1.133	+0.194(32)
H(82)	0.796(31)	1.230	0.000	1.133	+0.204(31)

Total charge in the ASU : +0.0001
Sum of monopoles in ASU : 144.2089

Table S6. Dipole Population Parameters.

Atom	D11+	D11-	D10	Kappa'
BR(1)	0.022(16)	-0.002(16)	0.030(16)	1.123
BR(2)	0.006(15)	-0.004(14)	0.074(15)	1.123
CU	0.000	0.000	0.000	1.012
CL(1)	-0.037(16)	0.020(17)	0.009(16)	0.986
CL(12)	-0.017(15)	0.042(16)	0.044(16)	0.986
CL(2)	0.031(17)	-0.018(16)	-0.043(17)	0.986
CL(22)	-0.012(15)	0.018(16)	-0.003(16)	0.986
N(1)	0.031(13)	-0.121(14)	-0.037(16)	0.903
N(2)	-0.002(14)	-0.123(14)	-0.071(16)	0.903
C(1)	-0.026(19)	0.004(22)	0.007(24)	0.952
C(12)	0.057(18)	0.049(21)	-0.078(24)	0.952
C(2)	0.074(20)	0.004(23)	-0.050(26)	0.952
C(22)	-0.006(19)	0.011(22)	-0.083(24)	0.952
C(3)	-0.015(17)	0.193(20)	-0.021(21)	0.952
C(32)	-0.016(17)	0.122(19)	0.062(21)	0.952
C(4)	0.009(17)	0.034(20)	-0.130(21)	0.952
C(42)	0.028(16)	0.002(19)	-0.055(20)	0.952
C(5)	-0.002(19)	0.053(24)	-0.069(25)	0.952
C(52)	-0.014(18)	0.005(23)	-0.024(24)	0.952
C(6)	-0.009(19)	-0.088(25)	-0.051(24)	0.952
C(62)	-0.025(19)	0.091(23)	-0.032(25)	0.952
C(7)	0.058(17)	0.014(21)	0.137(21)	0.952
C(72)	0.014(17)	0.123(19)	0.060(20)	0.952
C(8)	0.020(18)	0.023(22)	0.046(24)	0.952
C(82)	-0.029(18)	0.050(20)	-0.024(23)	0.952
C(9)	0.005(16)	-0.004(20)	-0.038(19)	0.952
C(92)	0.000	0.000	0.000(19)	0.952
H(1)	0.000	0.000	0.154(27)	1.133
H(12)	0.000	0.000	0.279(28)	1.133
H(2)	0.000	0.000	0.178(29)	1.133
H(22)	0.000	0.000	0.244(27)	1.133
H(5)	0.000	0.000	0.207(27)	1.133
H(52)	0.000	0.000	0.202(27)	1.133
H(6)	0.000	0.000	0.225(28)	1.133
H(62)	0.000	0.000	0.206(28)	1.133
H(8)	0.000	0.000	0.149(26)	1.133
H(82)	0.000	0.000	0.208(26)	1.133

Table S7. Quadrupole Population Parameters.

Atom	Q20	Q21+	Q21-	Q22+	Q22-	Kappa'
BR(1)	-0.067(18)	-0.120(16)	-0.140(16)	0.017(16)	0.028(16)	1.123
BR(2)	-0.139(17)	0.141(16)	0.035(15)	0.061(16)	0.022(16)	1.123
CU	-0.090(8)	0.028(8)	0.025(8)	0.008(8)	0.270(8)	1.012
CL(1)	-0.144(18)	0.051(17)	0.052(18)	-0.067(18)	0.047(18)	0.986
CL(12)	-0.102(17)	0.051(16)	-0.052(17)	-0.098(17)	-0.083(17)	0.986
CL(2)	-0.033(20)	0.000(18)	0.041(18)	-0.077(18)	-0.017(17)	0.986
CL(22)	-0.063(17)	0.057(16)	0.030(17)	-0.070(16)	0.052(16)	0.986
N(1)	0.130(16)	0.004(15)	-0.006(15)	-0.133(14)	-0.040(13)	0.903
N(2)	0.111(16)	-0.018(14)	0.044(15)	-0.138(14)	-0.004(13)	0.903
C(1)	0.190(21)	-0.006(18)	0.023(20)	-0.218(19)	-0.009(18)	0.952
C(12)	0.099(21)	-0.004(18)	0.016(20)	-0.250(18)	-0.026(18)	0.952
C(2)	0.139(23)	0.008(19)	-0.014(22)	-0.228(20)	-0.009(19)	0.952
C(22)	0.110(22)	-0.021(18)	-0.035(21)	-0.156(20)	0.009(19)	0.952
C(3)	0.145(22)	0.012(19)	-0.142(21)	-0.220(18)	-0.006(18)	0.952
C(32)	0.192(21)	0.034(18)	-0.066(20)	-0.139(17)	-0.033(16)	0.952
C(4)	0.065(21)	0.031(18)	-0.062(21)	-0.172(17)	-0.034(16)	0.952
C(42)	0.056(21)	0.012(18)	0.007(20)	-0.193(18)	0.062(17)	0.952
C(5)	0.140(23)	0.003(18)	-0.085(23)	-0.210(20)	-0.081(20)	0.952
C(52)	0.110(23)	-0.003(17)	-0.010(22)	-0.166(20)	0.067(19)	0.952
C(6)	0.073(23)	-0.006(18)	-0.085(24)	-0.236(22)	-0.020(21)	0.952
C(62)	0.096(23)	-0.070(18)	-0.008(23)	-0.171(20)	0.029(19)	0.952
C(7)	0.161(21)	0.051(18)	-0.063(21)	-0.139(19)	-0.006(18)	0.952
C(72)	0.154(21)	-0.024(17)	-0.110(20)	-0.129(18)	-0.034(16)	0.952
C(8)	0.119(22)	0.004(17)	-0.007(20)	-0.182(18)	0.013(18)	0.952
C(82)	0.080(21)	-0.039(17)	-0.039(20)	-0.226(18)	-0.020(17)	0.952
C(9)	0.077(19)	-0.001(16)	-0.058(19)	-0.251(18)	0.009(17)	0.952
C(92)	0.140(19)	-0.005(16)	-0.024(19)	-0.195(17)	-0.038(16)	0.952
H(1)	0.077(34)	-0.037(30)	-0.001(29)	-0.087(30)	0.004(29)	1.133
H(12)	0.209(34)	-0.005(29)	-0.046(29)	-0.030(29)	-0.010(28)	1.133
H(2)	0.106(36)	0.074(33)	-0.008(31)	0.008(30)	0.033(29)	1.133
H(22)	0.113(34)	-0.029(30)	0.027(30)	0.016(29)	-0.021(29)	1.133
H(5)	0.111(35)	-0.039(29)	0.026(31)	0.016(30)	-0.027(30)	1.133
H(52)	0.115(34)	-0.018(29)	-0.077(31)	0.037(29)	-0.008(28)	1.133
H(6)	0.083(34)	0.057(31)	0.045(31)	0.071(31)	-0.020(30)	1.133
H(62)	0.079(34)	-0.113(29)	-0.008(31)	0.050(30)	0.060(29)	1.133
H(8)	0.097(34)	0.018(29)	-0.019(30)	0.007(27)	-0.002(27)	1.133
H(82)	0.127(33)	-0.083(29)	0.023(29)	-0.015(27)	-0.056(27)	1.133

Table S8. Octupole Population Parameters.

Atom	O30	O31+	O31-	O32+	O32-	O33+	O33-	Kappa'
BR(1)	0.039(18)	0.005(17)	0.058(16)	-0.032(17)	-0.010(16)	0.030(16)	-0.038(16)	1.123
BR(2)	-0.010(16)	0.012(16)	-0.009(15)	0.025(16)	0.009(16)	-0.043(15)	-0.006(15)	1.123
CU	0.000	0.000	0.000	0.000	0.000	0.000	0.000	1.012
CL(1)	0.107(20)	-0.011(18)	-0.018(20)	-0.002(19)	-0.024(20)	0.004(21)	0.018(20)	0.986
CL(12)	0.166(19)	-0.011(17)	0.014(19)	0.038(18)	0.011(18)	-0.010(19)	-0.040(19)	0.986
CL(2)	0.152(22)	0.011(21)	0.005(20)	-0.022(20)	-0.019(20)	-0.011(19)	0.030(20)	0.986
CL(22)	0.155(19)	0.032(18)	-0.001(18)	-0.001(18)	0.012(18)	-0.007(17)	0.017(18)	0.986
N(1)	0.139(20)	-0.018(19)	0.008(21)	0.094(19)	-0.005(19)	-0.002(17)	-0.008(17)	0.903
N(2)	0.140(20)	-0.006(19)	0.011(20)	0.130(19)	0.030(18)	-0.007(17)	-0.034(18)	0.903
C(1)	0.281(27)	0.006(22)	0.073(26)	0.228(26)	-0.011(26)	0.011(25)	-0.002(24)	0.952
C(12)	0.256(27)	-0.006(22)	0.093(25)	0.187(26)	0.013(26)	-0.004(23)	-0.002(23)	0.952
C(2)	0.242(29)	0.005(24)	-0.016(28)	0.161(28)	0.060(28)	-0.028(25)	-0.003(25)	0.952
C(22)	0.278(28)	0.030(22)	-0.093(27)	0.169(26)	0.015(27)	-0.041(24)	-0.013(24)	0.952
C(3)	0.257(28)	0.007(25)	0.034(30)	0.260(26)	-0.086(25)	-0.009(23)	-0.005(23)	0.952
C(32)	0.207(28)	0.058(24)	-0.030(29)	0.184(25)	-0.017(24)	-0.001(21)	0.011(21)	0.952
C(4)	0.164(28)	0.003(25)	-0.019(31)	0.117(25)	0.040(25)	-0.009(22)	-0.006(21)	0.952
C(42)	0.240(27)	-0.018(23)	0.067(30)	0.174(24)	0.005(24)	-0.028(21)	0.004(21)	0.952
C(5)	0.269(29)	0.010(22)	0.038(29)	0.168(27)	0.009(28)	-0.014(25)	-0.016(25)	0.952
C(52)	0.244(28)	-0.014(21)	0.049(28)	0.067(27)	-0.005(26)	-0.018(24)	0.013(24)	0.952
C(6)	0.253(30)	0.045(22)	0.017(30)	0.147(28)	-0.011(29)	0.048(26)	0.061(26)	0.952
C(62)	0.290(29)	-0.046(22)	-0.025(28)	0.168(27)	0.015(27)	0.021(24)	0.001(25)	0.952
C(7)	0.276(28)	0.014(24)	0.012(30)	0.189(26)	0.026(26)	-0.010(24)	0.013(24)	0.952
C(72)	0.209(27)	0.031(23)	0.051(29)	0.157(24)	0.035(24)	0.017(22)	0.011(22)	0.952
C(8)	0.227(27)	0.028(21)	0.036(26)	0.150(25)	-0.008(25)	0.006(23)	-0.012(23)	0.952
C(82)	0.256(27)	0.024(21)	-0.037(26)	0.187(25)	-0.021(24)	0.008(22)	-0.015(22)	0.952
C(9)	0.332(26)	-0.008(22)	-0.023(29)	0.177(23)	0.016(23)	-0.018(22)	-0.056(22)	0.952
C(92)	0.280(26)	-0.024(22)	-0.064(29)	0.192(23)	-0.003(23)	-0.020(21)	-0.010(21)	0.952

Table S9. Hexadecapole Population Parameters.

Atom	H40	H41+	H41-	H42+	H42-	H43+	H43-	H44+	H44-	Kappa'	
BR(1)	0.060(21)	0.098(19)	-0.060(19)	-0.015(19)	0.060(19)	-0.074(18)	0.104(19)	-0.012(18)	0.005(17)	1.123	
BR(2)	0.059(20)	0.012(19)	-0.088(18)	0.065(19)	-0.008(19)	-0.005(19)	-0.081(19)	-0.006(18)	-0.045(18)	1.123	
CU	-0.133(15)	0.137(14)	-0.044(15)	0.080(15)	-0.007(15)	-0.011(15)	0.058(15)	-0.037(14)	0.070(14)	1.012	
CL(1)	0.128(24)	0.053(22)	-0.041(24)	0.014(23)	-0.061(23)	-0.054(25)	0.021(25)	-0.013(25)	-0.010(25)	0.986	
CL(12)	0.142(22)	0.062(20)	-0.026(22)	-0.025(22)	-0.018(22)	-0.035(22)	-0.015(23)	0.005(23)	-0.068(23)	0.986	
CL(2)	0.007(27)	0.009(25)	0.043(24)	-0.107(25)	-0.032(25)	0.006(25)	-0.065(24)	0.035(24)	-0.027(24)	0.986	
CL(22)	0.060(23)	0.020(21)	-0.021(22)	-0.005(22)	-0.014(21)	0.045(21)	0.001(21)	0.027(21)	-0.022(20)	0.986	

Section S2. Crystal packing

S2.1 Atom–atom contacts

Many experimental, computational and statistical studies have highlighted the involvement of halogen atoms in several interaction modes in organic crystals. [7]–[13] The nature of the specific interactions varies significantly based on the type of atom bonded to the halogen, be it a metal or a carbon, and that of the neighboring group. For example, the directional properties of M-X metal halides in their formation of hydrogen bonds have been exploited in crystal engineering,[14] while the C-X group can act as a weak hydrogen bond acceptor,[15],[16] as in CDCQB where C–H···Cl–C interactions are present. In the title compound, packing is assisted by both Cl···Cl and halogen···H contacts. In the absence of strong hydrogen bonds, the competition between X···X and X···H contacts (X = halogen) can indeed affect packing significantly.[17]

Table S10 below summarizes the most relevant symmetry–independent CH···X contacts. Those involving Br are likely the strongest ones, as they are partially charge–assisted due to the negative charge of bromine ligands.

Table S10. Halogen···hydrogen contacts of CDCQB at 100 K. Only contacts with distance lower than 3.0 Å and angle larger than 120 deg are shown. When meaningful, estimated standard deviations are given.

Interaction	H···X / Å	C···X / Å	C–H···X / deg	Symmetry
C(5)–H(5)···Br(2)	2.82	3.6124(6)	129.6	x, y, 1+z
C(12)–H(12)···Br(2)	2.88	3.7019(7)	133.0	1-x, 2-y, 1-z
C(62)–H(62)···Br(1)	2.70	3.6872(7)	151.7	-x, 1-y, 1-z
C(2)–H(2)···Cl(22)	2.74	3.4630(8)	123.8	x, 1+y, z

Intermolecular Cl···Cl contacts occur frequently in the packing of aromatic chlorinated compounds[18] and have been already observed in the crystalline packing of 2-chloroquinolinic compounds together with C–H···Cl ones.[19] As for CDCQB, type–I contacts[20] are set up between Cl(1) and Cl(12), forming a 1D–motif along approximately the [1 $\bar{1}$ 1] direction (Figure S7). Adjacent chains are connected along *b* by type–II halogen bonded contacts [20] involving atoms Cl(2) and Cl(12) (Figure S8). Numerical distances and angles are summarized in Table S11.

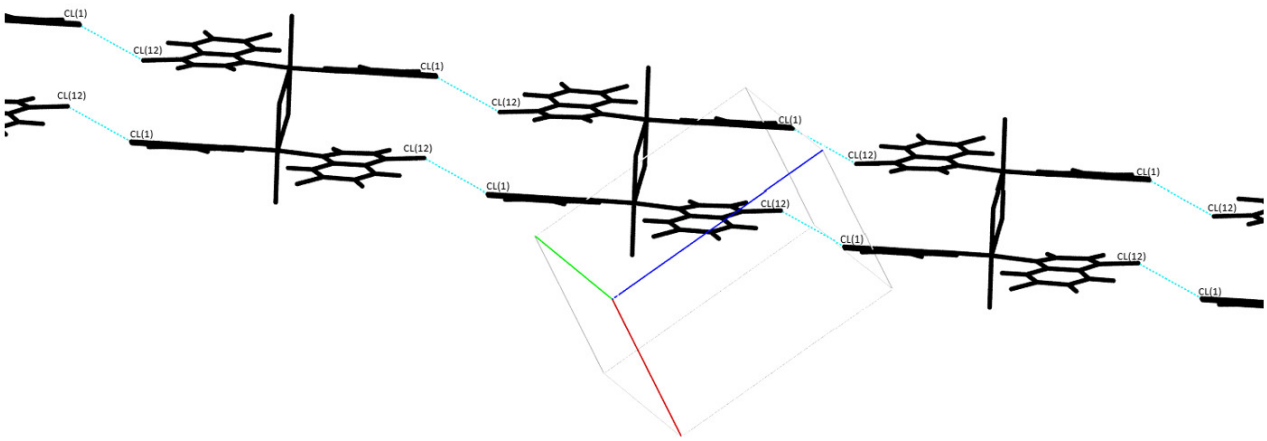

Figure S7. Type–I halogen bonded motif along [1 $\bar{1}$ 1] in CDCQB at 100 K. Cl(1)···Cl(12) contacts are highlighted as dashed light blue line.

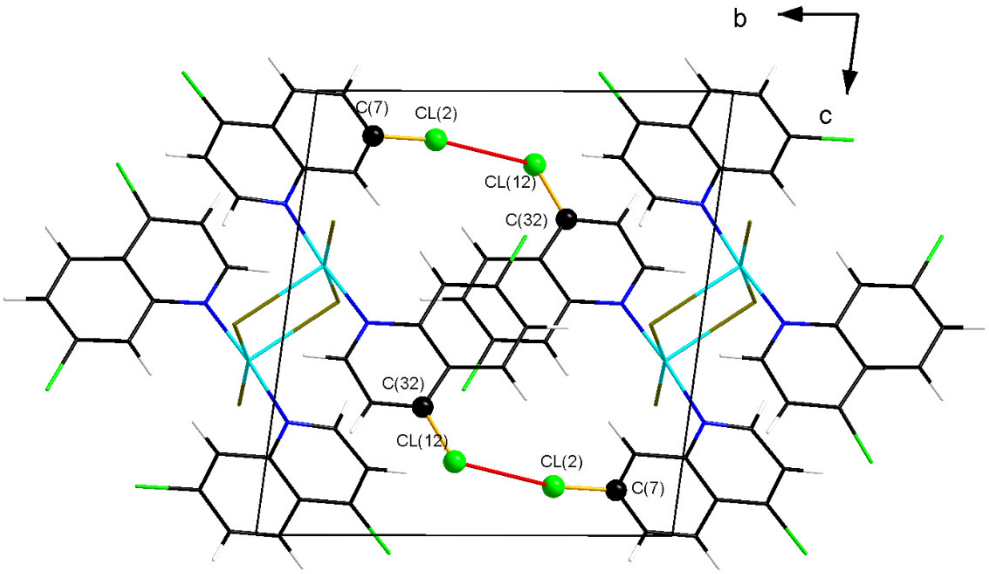

Figure S8. View of the unit cell of CDCQB at 100 K down the *a* axis, to show the type–II Cl(2)···Cl(12) contact (solid red lines) connecting organic dimers along *b*.

Table S11. Relevant geometrical parameters (Å, deg) for symmetry–independent halogen–bonded interactions in CDCQB at 100 K.

Interaction	Cl···Cl / Å	C–Cl···Cl / deg	Symmetry	Type
C(3)–Cl(1)···Cl(12)	3.2707(5)	154.58(3)	1-x, 1-y, 2-z	I
C(32)–Cl(12)···Cl(2)	3.6098(6)	107.73(3)	-x, 1-y, 1-z	II

S2.2 Stacking motifs

Each quinoline ring of DCQ participates in π–stacking interactions with translation–related aromatic rings. As each complex has four quinoline rings, as many adjacent metal centres are involved, forming an interesting 3D network dominated by π-stacking interactions (Figure S9). The latter are generally interpreted as a predominantly electrostatic (quadrupolar) in nature. Table S12 shows the distances between neighboring atoms belonging to the stacked rings, which lie in the typical range of similar interactions (3.4–3.8 Å). Figure S10 displays the interaction geometries for the two symmetry–independent rings (C1–C9, ring I; C12–C92, ring II) in the quinoline ligand. All the stacked ring are inversion–related (Figure S10), thus the mutual distances among their atoms are the same. An offset–stacked geometry is preferred, exploiting an offset angle of ~ 20 deg between the quinoline main planes.

Table S12. X-ray determined stacking distances at 100 K between facing rings of the quinoline ligands.

Rings*	Atoms	d(C···C) / Å
I–I	C3–C7	3.3168(9)
I–I	C5–C9	3.3664(8)
II–II	C42–C62	3.3949(9)

* See Figure S10 for definition of the rings and the atom numbering scheme.

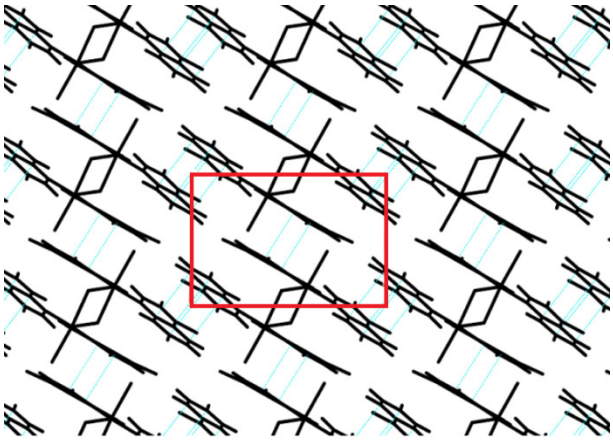

Figure S9. Crystal packing of CDCQB at 100 K, as viewed down the *b* axis, with the unit cell highlighted in red. π–stacking interactions between neighboring complexes are evident.

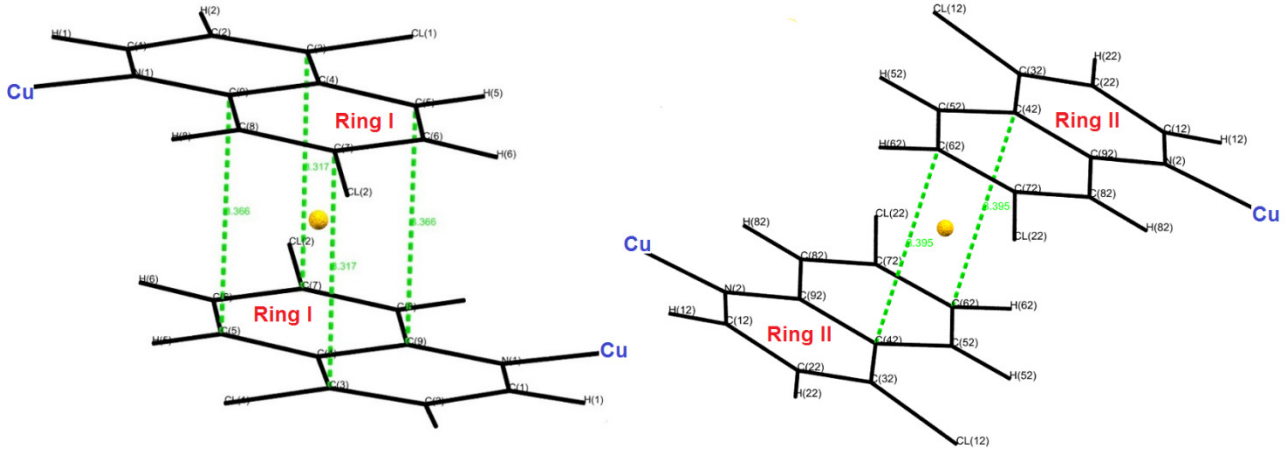

Figure S10. Atom and ring numbering for Table S12. The inversion symmetry is highlighted as a gold dot. Stacking distances are shown as green dashed lines.

Section S3. Geometry

S3.1 Coordination and relative ligand orientation

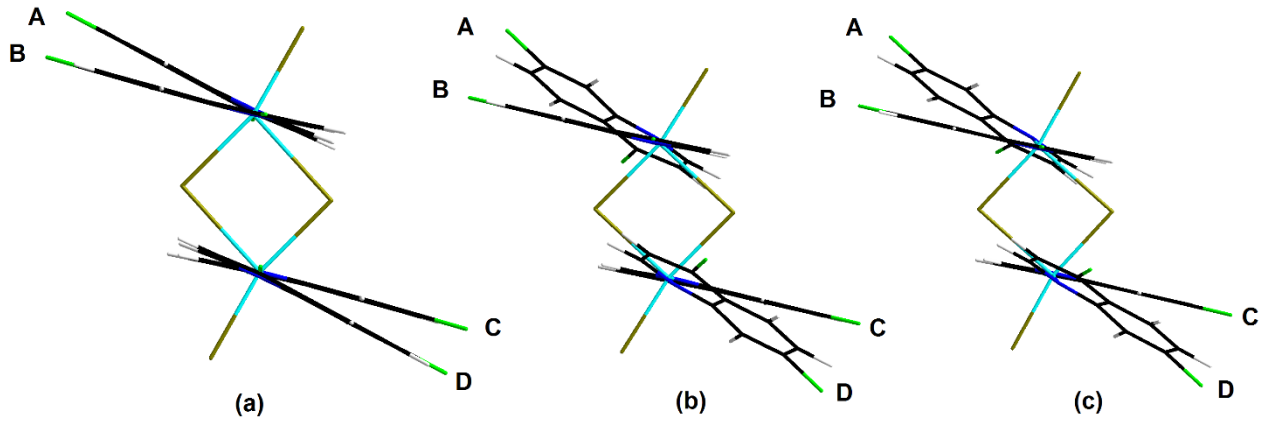

Figure S11. Comparison of X-ray (a) and *in vacuo* DFT–optimized ((b): singlet state; (c): triplet state) structures for the $[Cu(4,7–DCQ)_2Br_2]_2$ complex. Wires–stick representations are drawn approximately along the N–Cu–N directions. 4,7–dichloroquinoline ligands are labelled with capital letters. Dihedral angles between least–squares planes defined by backbone 4,7–DCQ C and N atoms are as follows: A–B: 12.6 deg (a), 21.9 deg (b) and 21.7 deg (c); A–C 12.6 (a), 21.9 deg (b) and 21.8 (c); A–D: 0.0 deg (a), 0.0 deg (b), and 1.2 deg (c).

Table S13. Coordination geometries (Å, deg) of multipole X–ray (T = 100 K) and *in vacuo* DFT–optimized (T = 0 K) structures, both in the singlet and triplet spin state, of CDCQB. Suffixes "eq" and "ap" stand for "equatorial" and "apical" positions.

Parameter	Experimental	DFT–optimized Singlet state	DFT–optimized Triplet state
$Cu–N(1)_{eq}$	2.0528(5)	2.002	2.018
$Cu–N(2)_{eq}$	2.0280(4)	1.992	2.004
$Cu–Br(1)_{eq}$	2.4519(2)	2.517	2.481
$Cu–Br(2)_{eq}$	2.4027(2)	2.386	2.375
$Cu–Br(1)_{ap}$	2.8056(2)	2.736	2.809
$N(1)_{eq}–Cu–N(2)_{eq}$	175.45(2)	169.7	171.3
$Br(1)_{eq}–Cu–Br(2)_{eq}$	164.31(1)	167.1	166.1
$N1(1)_{eq}–Cu–Br(1)_{eq}$	92.32(1)	92.1	92.3
$N1(1)_{eq}–Cu–Br(2)_{eq}$	89.91(1)	89.7	89.0
$N(2)_{eq}–Cu–Br(1)_{eq}$	88.78(1)	85.4	86.1
$N(2)_{eq}–Cu–Br(2)_{eq}$	87.85(1)	90.7	90.5
$N(1)_{eq}–Cu–Br(1)_{ap}$	91.64(2)	92.0	94.3
$N(2)_{eq}–Cu–Br(1)_{ap}$	92.83(1)	95.3	94.3
$Br(1)_{eq}–Cu–Br(1)_{ap}$	87.20(1)	91.8	91.2
$Br(2)_{eq}–Cu–Br(1)_{ap}$	108.27(1)	100.8	102.5

S3.2. DFT–optimized geometries

Table S14. DFT–optimized coordinates (Å) of the stoichiometric $Cu_2(4,7–DCQ)_4Br_4$ complex (singlet state). The complex is centrosymmetric and the full molecule can be retrieved by inverting the listed coordinates through the origin.

Center number	Atomic number	Label	X	Y	Z
1	35	Br1	-1.218407	-1.426276	-0.210028
2	35	Br2	3.127826	-0.903845	-2.348107
3	29	Cu	1.025186	-0.897778	-1.220479
4	17	CL1	-1.354243	2.289747	-6.378009
5	17	CL12	2.304973	-4.663753	3.856498
6	17	CL2	-2.372660	-4.264899	-4.120106
7	17	CL22	0.514480	-5.904915	-2.841004
8	7	N1	0.182246	-0.037495	-2.820335
9	7	N2	1.766763	-2.060145	0.217240
10	6	C1	0.578053	1.191450	-3.074369
11	6	C12	2.234050	-1.572688	1.340995
12	6	C2	0.141931	1.931993	-4.169417
13	6	C22	2.471272	-2.364304	2.464754
14	6	C3	-0.736777	1.348956	-5.017506
15	6	C32	2.169326	-3.683185	2.392288
16	6	C4	-1.176121	0.028334	-4.828973
17	6	C42	1.742561	-4.276646	1.193991
18	6	C5	-2.059279	-0.630069	-5.699701
19	6	C52	1.476735	-5.644973	1.021455
20	6	C6	-2.418969	-1.917586	-5.480225
21	6	C62	1.094064	-6.131238	-0.185583
22	6	C7	-1.892654	-2.584357	-4.373987
23	6	C72	0.982151	-5.254997	-1.268015
24	6	C8	-1.038561	-1.998262	-3.498501
25	6	C82	1.224088	-3.927897	-1.154899
26	6	C9	-0.668147	-0.659422	-3.695917
27	6	C92	1.586219	-3.406376	0.091578
28	1	H1	1.272595	1.623559	-2.361256
29	1	H12	2.387243	-0.497560	1.374743
30	1	H2	0.477062	2.949050	-4.319065
31	1	H22	2.834068	-1.916745	3.380453
32	1	H5	-2.436099	-0.090807	-6.559193
33	1	H52	1.588932	-6.306933	1.870621
34	1	H6	-3.095327	-2.440340	-6.143534
35	1	H62	0.886967	-7.183634	-0.331468
36	1	H8	-0.667837	-2.550889	-2.646709
37	1	H82	1.197425	-3.269166	-2.014128

Table S15. DFT–optimized coordinates (Å) of the stoichiometric $Cu_2(4,7–DCQ)_4Br_4$ complex (triplet state state). The inversion symmetry is broken, as the fully symmetric solution has led to imaginary frequencies in the nuclear part of the Hamiltonian, that is, does not correspond to a true topological minimum on the potential energy surface.

Center number	Atomic number	Label	X	Y	Z
1	35	Br1	0.677891	1.019839	1.430510
2	35	Br2	1.818820	1.632779	-3.211787
3	29	Cu	1.117604	1.086531	-1.009964
4	17	CL1	6.204154	-3.011111	-0.897431
5	17	CL12	-3.546232	5.492362	-0.165721
6	17	CL2	5.109370	3.152986	2.253003
7	17	CL22	3.478564	5.636073	0.254356
8	7	N1	2.719023	-0.128602	-0.837609
9	7	N2	-0.286216	2.514865	-1.084688
10	6	C1	2.701314	-1.230866	-1.557037
11	6	C12	-1.544663	2.252630	-1.345745
12	6	C2	3.757076	-2.137672	-1.605731
13	6	C22	-2.570907	3.167703	-1.113715
14	6	C3	4.860683	-1.865830	-0.871001
15	6	C32	-2.246499	4.367185	-0.573087
16	6	C4	4.955556	-0.703472	-0.088327
17	6	C42	-0.912573	4.730003	-0.329110
18	6	C5	6.081283	-0.368977	0.680835
19	6	C52	-0.496769	5.966866	0.190746
20	6	C6	6.122087	0.787214	1.385803
21	6	C62	0.819617	6.233226	0.380969
22	6	C7	5.026596	1.649390	1.330045
23	6	C72	1.766553	5.267127	0.031327
24	6	C8	3.912604	1.376688	0.606695
25	6	C82	1.419494	4.061745	-0.476945
26	6	C9	3.840446	0.174785	-0.112580
27	6	C92	0.063508	3.756714	-0.640893
28	1	H1	1.796001	-1.416840	-2.123630
29	1	H12	-1.759792	1.253815	-1.714938
30	1	H2	3.686847	-3.032736	-2.208001
31	1	H22	-3.597743	2.892312	-1.315927
32	1	H5	6.921567	-1.050879	0.692230
33	1	H52	-1.248289	6.706882	0.435104
34	1	H6	6.982310	1.058080	1.983903
35	1	H62	1.152862	7.181565	0.782135
36	1	H8	3.079341	2.065030	0.610001
37	1	H82	2.166057	3.353291	-0.813370
38	35	Br1A	-0.693386	-1.013708	-1.454126
39	35	Br2A	-1.831213	-1.664742	3.178969
40	29	CuA	-1.135312	-1.096529	0.982478
41	17	Cl1A	-6.186951	3.052129	0.955261
42	17	Cl12A	3.586490	-5.474259	0.240964
43	17	Cl2A	-5.170541	-3.090441	-2.264113

Center number	Atomic number	Label	X	Y	Z
44	17	Cl22A	-3.421521	-5.750481	-0.267393
45	7	N1A	-2.726084	0.140533	0.835514
46	7	N2A	0.273183	-2.522291	1.052245
47	6	C1A	-2.696504	1.231768	1.571335
48	6	C12A	1.523731	-2.243280	1.334908
49	6	C2A	-3.743308	2.147993	1.637103
50	6	C22A	2.565853	-3.147209	1.133817
51	6	C3A	-4.853440	1.896032	0.905294
52	6	C32A	2.266236	-4.357940	0.605293
53	6	C4A	-4.962885	0.744463	0.108615
54	6	C42A	0.941346	-4.740332	0.343224
55	6	C5A	-6.096889	0.426607	-0.655256
56	6	C52A	0.554128	-5.994798	-0.154998
57	6	C6A	-6.152355	-0.722808	-1.370323
58	6	C62A	-0.754529	-6.287942	-0.354569
59	6	C7A	-5.063255	-1.593937	-1.332798
60	6	C72A	-1.721823	-5.329573	-0.041954
61	6	C8A	-3.940114	-1.334792	-0.618749
62	6	C82A	-1.402924	-4.102902	0.434881
63	6	C9A	-3.854521	-0.142228	0.113430
64	6	C92A	-0.054063	-3.774093	0.617424
65	1	H1A	-1.788392	1.400175	2.138033
66	1	H12A	1.720738	-1.239078	1.699276
67	1	H2A	-3.661745	3.034156	2.251116
68	1	H22A	3.585190	-2.855861	1.350843
69	1	H5A	-6.932374	1.114401	-0.653138
70	1	H52A	1.321128	-6.727845	-0.370574
71	1	H6A	-7.019889	-0.982206	-1.962825
72	1	H62A	-1.067156	-7.252077	-0.734484
73	1	H8A	-3.107377	-2.023598	-0.634286
74	1	H82A	-2.166246	-3.396429	0.737278

Section S4. Chemical bonding

Table S16. Relevant bond critical point properties, according to the Quantum Theory of Atoms in Molecules,[21] in the copper coordination shell of the $[Cu(4,7–DCQ)_2Br_2]_2$ binuclear complex isolated from the crystal. "eq" and "ap" stand for "equatorial" and "apical" positions, respectively. Atom numbering is the same as in Figures 1 and 3 (main text). First row: experimental estimate, from the multipole model described in Sections S1.1–S1.3. Second row: Multipole–projected (F_{theo}) estimates from bulk DFT calculations, with full occupancy in the asymmetric unit (Section S1.4).

Bond →	$Cu–Br(1)_{eq}$	$Cu–Br(2)_{eq}$	$Cu–N(1)_{eq}$	$Cu–N(2)_{eq}$	$Cu–Br(1)_{ap}$
Distance X-Y / Å →	2.452	2.403	2.053	2.029	2.806
X–BCP [a] / Å	1.094	1.093	1.002	0.984	1.257
	1.124	1.114	1.003	0.994	1.270
BCP–Y [a] / Å	1.358	1.310	1.051	1.044	1.549
	1.328	1.289	1.050	1.032	1.536
ρ_{bcp} / e·Å^{-3}	0.36	0.36	0.54	0.60	0.18
	0.32	0.34	0.52	0.55	0.17
$\nabla^2\rho_{bcp}$ / e·Å^{-5}	4.35	4.28	7.49	8.24	2.04
	3.64	3.92	7.56	7.88	1.82
λ_1 [b] / e·Å^{-5}	-1.23	-1.28	-2.74	-3.15	-0.49
	-1.02	-1.03	-2.55	-2.75	-0.45
λ_2 [b] / e·Å^{-5}	-1.19	-1.20	-2.56	-2.87	-0.48
	-0.95	-0.95	-2.29	-2.47	-0.44
λ_3 [b] / e·Å^{-5}	6.77	6.76	12.79	14.26	3.01
	5.61	5.89	12.40	13.09	2.72
ε [c]	0.04	0.06	0.07	0.10	0.02
	0.08	0.08	0.11	0.11	0.03
$G(\mathbf{r})_{bcp}$ [d] / au	0.35	0.35	0.64	0.72	0.14
	0.29	0.32	0.62	0.66	0.13
$V(\mathbf{r})_{bcp}$ [d] / au	-0.39	-0.39	-0.75	-0.87	-0.14
	-0.33	-0.36	-0.72	-0.77	-0.13
$H(\mathbf{r})_{bcp}$ [d] / au	-0.04	-0.04	-0.11	-0.15	0.00
	-0.04	-0.04	-0.10	-0.11	0.00

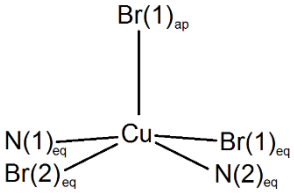

[a] Distance of the bond critical point (BCP) from X, Y atoms involved in the bonded pair.
[b] Charge density Hessian eigenvalues, $\lambda_1<\lambda_2<\lambda_3$ and $\lambda_1+\lambda_2+\lambda_3 = \nabla^2\rho_{bcp}$.
[c] Bond ellipticity, $\varepsilon = \lambda_1 / \lambda_2 – 1$
[d] Kinetic ($G(\mathbf{r})$), potential ($V(\mathbf{r})$) and total ($H(\mathbf{r})$) energy densities at the BCP, in atomic units (au).

Table S17. (3, –1) bond critical points as estimated from the experimental charge density of the $[Cu(4,7–DCQ)_2Br_2]_2$ complex at T = 100 K. See Table S16 for the meaning of the various quantities and Figure S12 for atom labels. Inversion–related atoms ara marked with "i". Energies in atomic units (au).

X	Y	X–BCP / Å	BCP-Y / Å	ρ_{bcp} /e·Å^{-3}	$\nabla^2\rho_{bcp}$ /e·Å^{-5}	ε	$G(\mathbf{r})_{bcp}$ / au	$V(\mathbf{r})_{bcp}$ / au	$H(\mathbf{r})_{bcp}$ / au
Br(1)	H(8)	1.074	1.772	0.06	0.94	1.08	0.05	-0.04	0.01
Br(1)	i_H(1)	1.033	1.698	0.08	1.06	0.48	0.06	-0.05	0.01
Br(1)	i_H(12)	0.918	1.706	0.08	0.71	0.71	0.05	-0.04	0.01
Cl(1)	i_Cl(12)	1.848	1.846	0.03	0.39	0.05	0.01	-0.01	0.00
N(1)	i_C(12)	1.804	1.865	0.02	0.20	0.37	0.01	-0.01	0.00
C(3)	i_C(22)	1.913	1.953	0.02	0.22	0.52	0.01	-0.01	0.00
C(3)	C(2)	0.676	0.696	2.30	-22.72	0.23	2.16	-5.91	-3.75
C(3)	Cl(1)	0.739	0.977	1.46	-5.32	0.17	1.27	-2.90	-1.64
C(22)	C(32)	0.669	0.703	2.32	-22.75	0.25	2.20	-5.99	-3.79
C(32)	Cl(12)	0.716	1.006	1.46	-4.81	0.01	1.28	-2.90	-1.62
C(7)	C(6)	0.687	0.725	2.11	-19.26	0.18	1.89	-5.13	-3.24
C(7)	CL(2)	0.757	0.973	1.42	-3.02	0.06	1.31	-2.82	-1.52
C(62)	C(72)	0.677	0.734	2.12	-18.76	0.24	1.94	-5.20	-3.26
C(72)	Cl(22)	0.724	1.006	1.36	-2.37	0.11	1.23	-2.62	-1.39
C(72)	C(82)	0.672	0.700	2.39	-23.33	0.18	2.34	-6.31	-3.97
C(1)	N(1)	0.547	0.781	2.53	-28.63	0.08	2.43	-6.87	-4.44
C(4)	C(9)	0.687	0.741	1.95	-14.44	0.21	1.77	-4.54	-2.78
C(8)	C(9)	0.656	0.760	2.13	-19.57	0.19	1.93	-5.24	-3.30
C(9)	N(1)	0.603	0.772	2.25	-20.19	0.07	2.15	-5.72	-3.57
H(1)	C(1)	0.349	0.735	1.98	-21.90	0.02	1.49	-4.50	-3.02
C(12)	N(2)	0.568	0.758	2.58	-26.39	0.09	2.66	-7.18	-4.51
C(92)	C(42)	0.701	0.723	2.13	-18.43	0.21	1.97	-5.23	-3.26
C(82)	C(92)	0.694	0.718	2.13	-19.24	0.20	1.94	-5.22	-3.28
C(92)	N(2)	0.613	0.761	2.34	-20.06	0.11	2.39	-6.19	-3.80
H(12)	C(12)	0.399	0.684	2.07	-27.02	0.03	1.43	-4.76	-3.32
C(1)	C(2)	0.703	0.703	2.21	-20.57	0.15	2.05	-5.55	-3.49
H(2)	C(2)	0.362	0.721	1.90	-21.48	0.04	1.34	-4.19	-2.85
C(22)	C(12)	0.686	0.721	2.12	-19.40	0.22	1.91	-5.18	-3.27
H(22)	C(22)	0.377	0.707	1.93	-23.99	0.10	1.29	-4.26	-2.97
C(4)	C(3)	0.589	0.827	2.08	-19.12	0.10	1.83	-5.00	-3.17
C(42)	C(32)	0.687	0.733	2.02	-16.54	0.16	1.82	-4.80	-2.98
C(5)	C(4)	0.686	0.731	2.02	-15.57	0.16	1.88	-4.84	-2.97
C(52)	C(42)	0.687	0.731	2.04	-15.48	0.19	1.92	-4.92	-3.00
H(5)	C(5)	0.374	0.709	1.98	-23.09	0.06	1.43	-4.47	-3.04
C(6)	C(5)	0.653	0.716	2.39	-24.10	0.24	2.31	-6.32	-4.00
H(6)	C(6)	0.396	0.688	1.90	-20.80	0.09	1.38	-4.22	-2.84
H(8)	C(8)	0.360	0.723	1.88	-19.76	0.05	1.37	-4.13	-2.76
C(52)	C(62)	0.662	0.712	2.22	-19.35	0.24	2.14	-5.64	-3.50
H(62)	C(62)	0.372	0.711	1.95	-22.09	0.11	1.41	-4.36	-2.95
H(82)	C(82)	0.372	0.711	1.94	-22.79	0.05	1.35	-4.30	-2.95
C(8)	C(7)	0.641	0.734	2.32	-23.51	0.15	2.18	-6.01	-3.83
H(8)	H(82)	1.047	1.130	0.06	0.22	0.23	0.02	-0.02	0.00

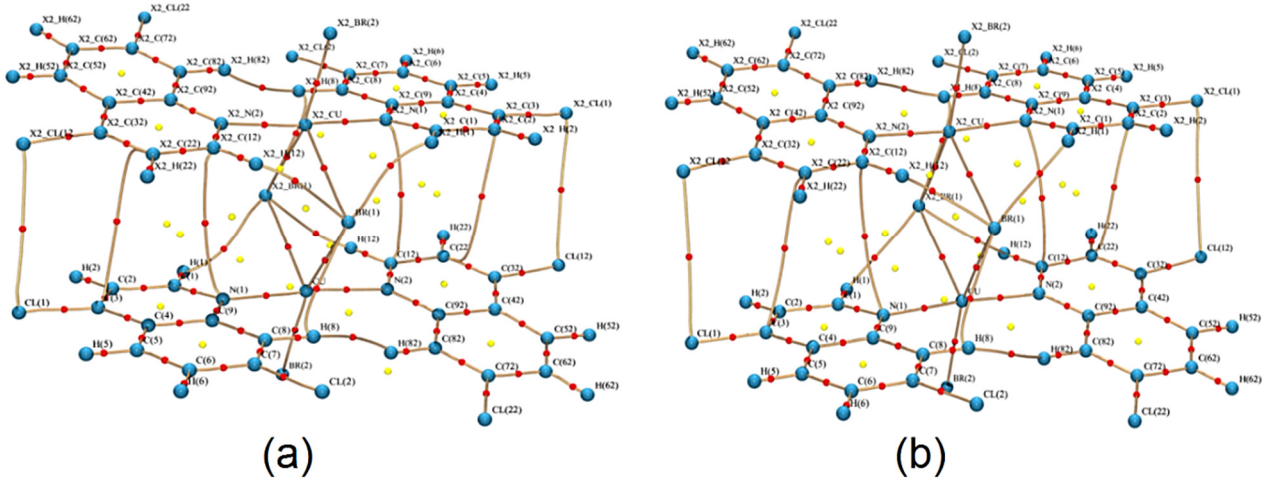

Figure S12. Molecular graph of $[Cu(4,7–DCQ)_2Br_2]_2$ at 100 K, as determined from the analysis of the gradient vector field of experimental (F_{exp}) (a) and multipole–projected DFT (F_{theo}) (b) electron densities. Each line represents a full atomic interaction line (AIL) between pairs of topologically bonded atoms, that is, a path of maximum density joining two (3, –3) nuclear attractors. As shown by Bader,[22] the set of AILs is homeomorphic with the molecular virial field and denotes attractive interactions between neighboring atoms. Red (yellow) points mark bond (ring) critical points. Table S17 reports on the corresponding numerical quantities for experimental bond critical points.

S4.1 Aromaticity of 4,7–dichloroquinoline

Several descriptors of aromaticity are available, lying either on quantum–mechanical or geometrical grounds,[23] which in most cases correlate to each other.[24–26] We here resort to HOMED (Harmonic Oscillator Model of Electron Delocalization),[27] which has been also recently applied to solid–state studies, [28] which can be computed from the knowledge of accurate bond lengths in 4,7–dichloroquinoline moiety (Table S18). Similarly to its parent HOMA,[29] HOMED is widely and successfully employed in heterocyclic chemistry[30,31] as a geometric–based aromaticity index.

Table S18. Bond lengths (Å) of symmetry–independent 4,7–DCQ ligand, as estimated from the X–ray multipole model at T = 100 K and DFT simulations in the gas phase.

Bond	X-ray	Isolated complex, DFT (singlet)[a]	Isolated complex, DFT (triplet)[a]	Isolated ligand, DFT[a]	Ring[b]
N(1) - C(1)	1.327	1.316	1.316	1.306	R2
N(1) - C(9)	1.375	1.370	1.369	1.360	R2
C(1) - C(2)	1.405	1.392	1.392	1.401	R2
C(2) - C(3)	1.372	1.353	1.353	1.353	R2
C(3) - C(4)	1.417	1.405	1.405	1.403	R2
C(4) - C(9)	1.428	1.420	1.420	1.417	R1/R2
C(4) - C(5)	1.417	1.404	1.404	1.404	R1
C(5) - C(6)	1.368	1.355	1.355	1.356	R1
C(6) - C(7)	1.412	1.395	1.395	1.397	R1
C(7) - C(8)	1.375	1.356	1.356	1.353	R1
C(8) - C(9)	1.416	1.403	1.403	1.404	R1
N(2) - C(12)	1.325	1.311	1.312	1.306	R2
N(2) - C(92)	1.373	1.364	1.364	1.360	R2
C(12) - C(22)	1.407	1.395	1.394	1.401	R2
C(22) - C(32)	1.371	1.355	1.355	1.353	R2
C(32) - C(42)	1.420	1.404	1.404	1.403	R2
C(42) - C(92)	1.423	1.413	1.413	1.417	R1/R2
C(42) - C(52)	1.418	1.405	1.405	1.404	R1
C(52) - C(62)	1.373	1.356	1.357	1.356	R1
C(62) - C(72)	1.411	1.397	1.397	1.397	R1
C(72) - C(82)	1.372	1.354	1.353	1.353	R1
C(82) - C(92)	1.413	1.399	1.400	1.404	R1

[a] DFT–optimized structures in the gas phase. See Methods in the main text for details.
[b] Ring number (see Figure S10). R2 is the N–bearing ring and connected to copper through a coordinative bond. Bonds marked as R1/R2 are shared between the two quinoline rings.

Section S5. Magnetic susceptivity measurement

Table S19. Measured quantities on the Evans balance employed to derive magnetic susceptivity of the title compound, based on the Gouy method.[32] The mass susceptivity in cm^3/g is obtained from $\chi_g = CL\,(R_0 - R_s)/(10^9 \cdot m)$, C being the calibration constant, L the sample length, R_0 and R_s the readings, and m the sample mass. Diamagnetic corrections have been applied (Table S20).

Variable	Value	Measure units
L (sample length)	1.8	cm
m(test tube, empty)	0.7597	g
m(test tube+sample)	0.8792	g
m(sample)	0.1195	g
R_0 (test tube)	-31	cm
R_s (test tube+sample)	71	cm
ΔR (sample)	102	cm
C (calibration constant)	1.055063913	
T	291.75	K
Molecular weight	1220.80	g/mol
χ_g (mass susceptivity)	$1.621 \cdot 10^{-6}$	emu/g
χ_M (molar susceptivity)	$1.979 \cdot 10^{-6}$	emu/mol
χ'_M (molar susceptivity, corrected for diamagnetic contributions)	$2.614 \cdot 10^{-3}$	emu/mol
μ_{eff} (effective magnetic moment)	2.47	Bohr magnetons

Table S20. Pascal constants for diamagnetic corrections (x 10^{-6} emu/mol), from Bain & Berry.[33]

Chemical specie	Pascal Constants
Atoms	
C	-6.24
H	-2.93
N(ring)	-4.61
Cl	-20.1
Ions	
Cl^-	-23.4
Br^-	-34.6
Cu(II)	-11
Bonds	
Ar-Cl	-2.5
Benzene	-1.4
Pyridine	0.5

Section S6. DFT electronic structure

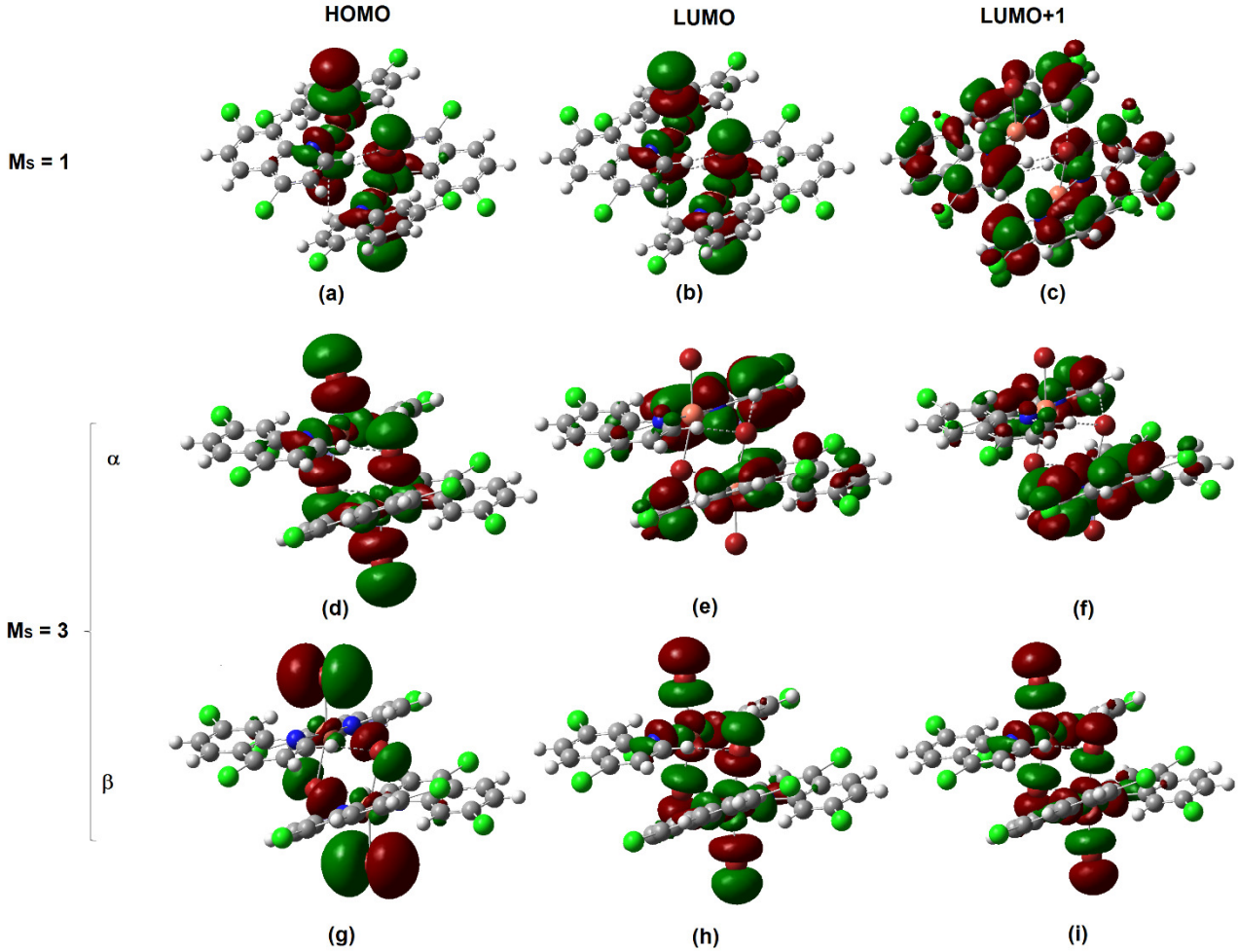

Figure S13. See also Figure 6 in the main text. Frontier orbitals of the binuclear $[Cu(4,7–DCQ)_2Br_2]_2$ complex. Cu: pink; Br: brown; Cl: green; C: grey; H: white; N: blue. 0.02 au–level isosurfaces are shown, with green (red) lobes representing positive (negative) orbital phases. Singlet (M_S = 1, (a)–(c)) and triplet (M_S = 3, (d)–(i)) spin states are considered, highlighting orbitals occupied by either α ((d)–(f)) and β ((g)–(i)) electrons. In both cases, the virtual states bear a significant π* contribution from quinoline ligands, while the highest occupied orbitals have a non–negligible metal character. The β HOMO involves the metal d_{z^2} orbital with a somewhat intermediate σ/π symmetry, while the α one is clearly σ–type and involves $d_{x^2-y^2}$ metal states. Energies are as follows (au). M_S=0: HOMO: -0.17882; LUMO: -0.13962; LUMO+1: -0.07525. M_S=3, α: HOMO: -0.22332; LUMO: -0.07523; LUMO+1: -0.07488. M_S=3, β: HOMO: -0.23010; LUMO: -0.09771; LUMO+1: -0.09277. The β LUMO+2 (not shown), has energy -0.07450 au and again bears main π* contribution from quinoline ligands.

Table S21. Mulliken atomic charges of the $[Cu(4,7–DCQ)_2Br_2]_2$ complex, as estimated from DFT calculations *in vacuo*, either at the same multipole–derived X-ray geometry at 100 K or at the fully relaxed geometry in both singlet and triplet spin state. Two-digit marks of atom labels refer to part of the molecule which in the solid state is inversion–dependent.

Atom	X-ray geometry [a]	DFT–optimized, singlet [a]	DFT–optimized, triplet [b]	
Br1	-0.781	-0.780	-0.805	-0.803
Br2	-0.695	-0.681	-0.711	-0.712
Cu	1.298	1.309	1.375	1.373
Cl1	-0.200	-0.208	-0.208	-0.208
Cl2	-0.212	-0.219	-0.218	-0.218
N1	-0.760	-0.797	-0.798	-0.798
C1	0.355	0.337	0.336	0.336
C2	-0.065	-0.047	-0.049	-0.049
C3	0.176	0.173	0.175	0.175
C4	-0.009	-0.014	-0.012	-0.013
C5	-0.011	-0.008	-0.008	-0.008
C6	-0.008	-0.005	-0.005	-0.005
C7	0.160	0.164	0.164	0.165
C8	0.035	0.019	0.019	0.018
C9	0.357	0.356	0.354	0.354
H1	0.076	0.085	0.085	0.086
H2	0.065	0.076	0.076	0.076
H5	0.056	0.060	0.060	0.060
H6	0.061	0.064	0.064	0.064
H8	0.015	0.038	0.038	0.038
Cl12	-0.192	-0.215	-0.216	-0.216
Cl22	-0.209	-0.222	-0.222	-0.222
N2	-0.787	-0.751	-0.758	-0.760
C12	0.354	0.343	0.344	0.345
C22	-0.056	-0.055	-0.056	-0.055
C32	0.167	0.172	0.175	0.175
C42	-0.009	0.002	0.001	0.001
C52	-0.013	-0.007	-0.007	-0.007
C62	-0.009	-0.005	-0.005	-0.005
C72	0.156	0.171	0.171	0.171
C82	0.018	0.008	0.006	0.007
C92	0.352	0.360	0.360	0.360
H12	0.079	0.072	0.072	0.072
H22	0.070	0.048	0.046	0.047
H52	0.058	0.058	0.058	0.058
H62	0.060	0.063	0.063	0.063
H82	0.045	0.033	0.035	0.035

[a] Inversion symmetry has been exploited. Only symmetry–independent atoms are shown.

[b] The inversion symmetry is broken, as the fully symmetric solution has led to imaginary frequencies in the nuclear part of the Hamiltonian, that is, does not correspond to a true topological minimum on the potential energy surface. All atoms are now symmetry–independent and must be reported.

References

1. Lo Presti, L.; Sist, M.; Loconte, L.; Pinto, A.; Tamborini, L.; Gatti, C. Rationalizing the lacking of inversion symmetry in a noncentrosymmetric polar racemate: An experimental and theoretical study. *Cryst. Growth Des.* **2014**.
2. Destro, R.; Ruffo, R.; Roversi, P.; Soave, R.; Loconte, L.; Lo Presti, L. Anharmonic motions versus dynamic disorder at the Mg ion from the charge densities in pyrope (Mg3Al2Si3O12) crystals at 30 K: Six of one, half a dozen of the other. *Acta Crystallogr. Sect. B Struct. Sci. Cryst. Eng. Mater.* **2017**, *73*, 722–736.
3. Herbst-Irmer, R.; Henn, J.; Holstein, J.J.; Hübschle, C.B.; Dittrich, B.; Stern, D.; Kratzert, D.; Stalke, D. Anharmonic motion in experimental charge density investigations. *J. Phys. Chem. A* **2013**.
4. Mallinson, P.R.; Koritsanszky, T.; Elkaim, E.; Li, N.; Coppens, P. The Gram–Charlier and multipole expansions in accurate X□ray diffraction studies: can they be distinguished? *Acta Crystallogr. Sect. A* **1988**.
5. Kuhs, W.F. Generalized atomic displacements in crystallographic structure analysis. *Acta Crystallogr. Sect. A* **1992**.
6. Su, Z.; Coppens, P. Nonlinear Least-Squares Fitting of Numerical Relativistic Atomic Wave Functions by a Linear Combination of Slater-Type Functions for Atoms with Z = 1–36. *Acta Crystallogr. Sect. A Found. Crystallogr.* **1998**, *54*, 646–652.
7. Brammer, L.; Bruton, E.A.; Sherwood, P. Understanding the Behavior of Halogens as Hydrogen Bond Acceptors. *Cryst. Growth Des.* **2001**.
8. Robertson, P.A.; Villani, L.; Dissanayake, U.L.M.; Duncan, L.F.; Abbott, B.M.; Wilson, D.J.D.; Robertson, E.G. Halocarbons as hydrogen bond acceptors: A spectroscopic study of haloethylbenzenes (PhCH2CH2X, X = F, Cl, Br) and their hydrate clusters. *Phys. Chem. Chem. Phys.* **2018**.
9. Neve, F.; Crispini, A. N,N -Dodecamethylene-bis(pyridinium) goes lamellar. Role of C-H□I, C-H□M, and I□I interactions in the crystal structure of its hexaiododipalladate(II) derivative. *CrystEngComm* **2003**.
10. Banerjee, R.; Desiraju, G.R.; Mondal, R.; Howard, J.A.K. Organic chlorine as a hydrogen-bridge acceptor: Evidence for the existence of intramolecular O-H□Cl-C interactions in some gem-alkynols. *Chem. - A Eur. J.* **2004**.
11. Taylor, R.; Kennard, O. Crystallographic Evidence for the Existence of C-H□O, C-H□N, and C-H□Cl Hydrogen Bonds. *J. Am. Chem. Soc.* **1982**.
12. McBride, M.T.; Luo, T.J.M.; Tayhas R Palmore, G. Hydrogen-bonding interactions in crystalline solids of cyclic thioureas. *Cryst. Growth Des.* **2001**.
13. Gavezzotti, A.; Lo Presti, L. Building Blocks of Crystal Engineering: A Large-Database Study of the Intermolecular Approach between C–H Donor Groups and O, N, Cl, or F Acceptors in Organic Crystals. *Cryst. Growth Des.* **2016**, *16*, 2952–2962.
14. Mareque Rivas, J.C.; Brammer, L. Self-Assembly of 1-D Chains of Different Topologies Using the Hydrogen-Bonded Inorganic Supramolecular Synthons N−H···Cl $_2$ M or N−H···Cl $_3$ M. *Inorg. Chem.* **1998**.
15. Aullón, G.; Bellamy, D.; Brammer, L.; Bruton, E.A.; Orpen, A.G. Metal-bound chlorine often accepts hydrogen bonds. *Chem. Commun.* **1998**.
16. Lewis, G.R.; Orpen, A.G. A metal-containing synthon for crystal engineering: Synthesis of the hydrogen bond ribbon polymer [4,4′-H2bipy][MCl4] (M = Pd, Pt). *Chem. Commun.* **1998**.
17. Destro, R.; Sartirana, E.; Loconte, L.; Soave, R.; Colombo, P.; Destro, C.; Lo Presti, L. Competing C=O???C=O, C-H???O, Cl???O, and Cl???Cl interactions governing the structural phase transition of 2,6-dichloro-p- benzoquinone at T c = 122.6 K. *Cryst. Growth Des.* **2013**, *13*, 4571–4582.

18. Sarma, J.A.R.P.; Desiraju, G.R. *The Role of Cl…Cl and C-H…O Interactions in the Crystal Engineering of 4-A Short-Axis Structures*; 1986;
19. Hathwar, V.R.; Mohana Roopan, S.; Subashini, R.; Nawaz Khan, F.; Guru Row, T.N. Analysis of Cl-Cl and C-H-Cl intermolecular interactions involving chlorine in substituted 2-chloroquinoline derivatives. In Proceedings of the Journal of Chemical Sciences; 2010.
20. Desiraju, G.R.; Parthasarathy, R. The Nature of Halogen•••Halogen Interactions: Are Short Halogen Contacts Due to Specific Attractive Forces or Due to Close Packing of Nonspherical Atoms? *J. Am. Chem. Soc.* **1989**.
21. Bader, R.F.W. *Atoms in Molecules: A Quantum Theory, International Series of Monographs on Chemistry 22*; 1990; ISBN 9780198558651.
22. Bader, R.F.W. Atoms in Molecules: A Quantum Theory, International Series of Monographs on Chemistry 22. *Oxford Univ. Press. Oxford Henkelman G, Arnaldsson A, Jónsson H A fast robust algorithm Bader Decompos. Charg. density. Comput Mater Sci* **1990**.
23. Monza, E.; Gatti, C.; Lo Presti, L.; Ortoleva, E. Revealing electron delocalization through the source function. *J. Phys. Chem. A* **2011**, *115*, 12864–12878.
24. Dobrowolski, J.C. Three Queries about the HOMA Index. *ACS Omega* **2019**.
25. Mollania, F.; Raissi, H. Theoretical study of substituents effects on characteristics of resonance-assisted hydrogen bond in (Z)-(thionitrosomethylene)hydrazine and its derivatives in ground and electronic excited state. *Struct. Chem.* **2014**.
26. Balaban, A.T.; Durdević, J.; Gutman, I.; Jeremić, S.; Radenković, S. Correlations between local aromaticity indices of bipartite conjugated hydrocarbons. *J. Phys. Chem. A* **2010**.
27. Raczyńska, E.D.; Hallman, M.; Kolczyńska, K.; Stepniewski, T.M. On the Harmonic Oscillator Model of Electron Delocalization (HOMED) index and its application to heteroatomic π-electron systems. *Symmetry (Basel).* **2010**.
28. Majerz, I.; Dziembowska, T. Aromaticity of benzene derivatives: an exploration of the Cambridge Structural Database. *Acta Crystallogr. Sect. B Struct. Sci. Cryst. Eng. Mater.* **2018**.
29. Krygowski, T.M.; Cyrański, M.K. Structural aspects of aromaticity. *Chem. Rev.* 2001.
30. Frizzo, C.P.; Martins, M.A.P. Aromaticity in heterocycles: New HOMA index parametrization. *Struct. Chem.* **2012**.
31. Katritzky, A. *Advances in Heterocyclic Chemistry. Heterocyclic Chemistry in the 21st Century - A Tribute to Alan Katritzky. Vol 115*; 2016; ISBN 9780128046951.
32. Atkins, P.W.; Overton, T.L.; Rourke, J.P.; Weller, M.T. *Shriver and Atkins' Inorganic Chemistry, Fifth Edition*; 2010;
33. Bain, G.A.; Berry, J.F. Diamagnetic Corrections and Pascal's Constants. *J. Chem. Educ.* **2008**, *85*, 532.